Linear Relationship between Deformability and Thermal Stability of 2′-*O*-Modified RNA Hetero Duplexes

Yoshiaki Masaki, Ryuta Miyasaka, Akihiro Ohkubo, Kohji Seio, and Mitsuo Sekine*

Department of Life Science, Tokyo Institute of Technology, 4259 Nagatsuta-cho, Midori-ku, Yokohama, Japan

Received: October 14, 2009; Revised Manuscript Received: November 19, 2009

We describe the relationship between the experimentally determined melting temperatures of 2′-*O*-modified-RNA/RNA duplexes and their deformability estimated from molecular dynamics simulations. To clarify this relationship, we synthesized several fully modified oligoribonucleotides such as 2′-*O*-cyanoethyl RNAs and 2′-*O*-methoxyethyl RNAs and compared the actual melting temperatures of the duplexes with their calculated deformabilities. An increase of the melting temperatures by 2′-*O*-modifications was found to correlate strongly with an increase of the helical elastic constants in U_{14}/A_{14}, $(CU)_7/(AG)_7$, and $(GACU)_3/(AGUC)_3$ sequences. Linear regression analyses could be used to estimate the melting temperature with an accuracy of ±2.0 °C in our model case. Although the strong correlation was observed in the same base sequence, the linear regression functions were different from each base sequence. Our results indicated the possibility of predicting the thermal stability of 2′-*O*-modified duplexes at the computer-aided molecular design stage.

Introduction

Chemical modification of natural RNAs has been of great importance in improving their original physicochemical and biochemical properties. Since RNAs are rapidly degraded by cellular nucleases, a large number of 2′-*O*-modified RNAs have been developed and applied to the gene regulation in antisense, antigene, and RNA interference (RNAi) strategies.[1−5] We are interested in 2′-*O*-alkyl-type modifications because they can enhance both hybridization affinity and the nuclease resistances. In contrast, it is reported that other modifications such as 2′-F modification increased the hybridization affinity but not enhance the nuclease resistance in comparison with unmodified DNA.[6] As one such 2′-*O*-modified RNA, we reported 2′-*O*-cyanoethylated RNA that showed enhanced hybridization affinity and nuclease resistance compared with 2′-*O*-methyl RNA.[7,8]

Currently, there is no method of predicting the hybridization properties of 2′-*O*-modified-RNAs, and they can be determined only experimentally, using actually synthesized 2′-*O*-modified-RNA samples. However, comparative studies among various 2′-*O*-modified RNAs are, in general, laborious and time-consuming tasks because it is sometimes difficult to synthesize certain 2′-*O*-modified nucleosides. Thus, a facile computational method for predicting thermal stability is eagerly anticipated for the efficient design of new 2′-*O*-modified-RNAs.

The effect of 2′-*O*-modification on the stability of RNA duplexes has been studied especially for the 2′-*O*-methyl group.[9−20] The stabilizing effect by the 2′-*O*-methyl group was commonly explained by the rigidity of the sugar puckering.[9−11] The rigid sugar puckering suppresses the entropy loss to form a duplex from the single strand.[21] ^{1}H NMR studies showed that the 2′-*O*-methylation of dinucleoside monophosphate derivatives increased the population of the *C3′-endo* form except for adenosine derivatives.[10] Circular dichroism (CD) studies also showed that the 2′-*O*-methylation increased the intensity of CD spectra in the dinucleoside monophosphates except for the adenine derivatives.[15,16]

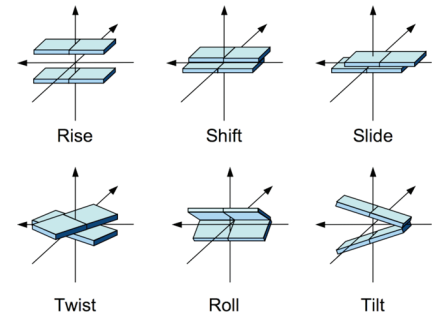

Figure 1. Pictorial definitions of parameters that relate sequential base-pair steps. The parameter values were calculated using the X3DNA software package.[40]

However, sugar puckering is not the ideal indicator. Although 2′-*O*-cyanoethylation apparently increased the T_m values of modified RNA duplexes more than 2′-*O*-methylation as reported by us, little difference was found in the population of the *C3′-endo* form between the 2′-*O*-cyanoethyl and 2′-*O*-methyl nucleosides by our ^{1}H NMR analysis.[7]

Recently, in addition to these conformational effects, the hydration shell has also been considered to play an important role in the 2′-*O*-methyl RNA/2′-*O*-methyl RNA homo duplex stability.[17,18]

The concept of deformability was widely used to evaluate the thermodynamic properties of nucleic acids, such as nucleosome folding, elasticity of rRNA, and RNaseH susceptibility.[22−30] De Santis and co-workers reported that the relative rigidities of several kinds of base pair steps in DNA and normalized melting temperatures are strongly correlated.[28−30] However, no research has estimated the effect of 2′-*O*- modification of RNAs by using the deformability.

In this paper, we show the relationship between the melting temperatures (T_m) of duplexes (U_{14}/A_{14}, $(CU)_7/(AG)_7$, and $(GACU)_3/(AGUC)_3$) and their deformabilities (sugar puckering, twist, roll, tilt, rise, shift, and slide) that are inferred from molecular dynamic simulations (Figure 1). The chemical structures of 2′-*O*-modified nucleosides used in this study are

* Corresponding author. Tel.: +81-45-924-5706. Fax: +81-45-924-5772. E-mail address: msekine@bio.titech.ac.jp.

10.1021/jp909851j
Published on Web 01/28/2010

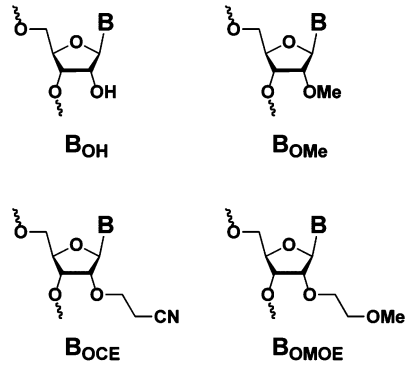

Figure 2. Chemical structures of 2′-*O*-modified nucleotides.

shown in Figure 2. We demonstrated that the deformability of the rise parameter correlates well with the melting temperature. This result suggested that the rigidity of the rise parameter, rather than the frequently discussed sugar puckering, could be a good indicator of the thermal stability changed by 2′-*O*-modification. Our results also showed a stronger correlation between the total stiffness indexes and the experimental T_m values. This means a new possibility of predicting the thermal stability of 2′-*O*-modified RNA/RNA duplexes at the molecular design stage.

Results

Synthesis of 2′-O-Modified Oligoribonucleotides. First, we synthesized oligoribonucleotides having 2′-*O*-modified nucleoside residues such as 2′-*O*-cyanoethyluridine (U_{OCE}), 2′-*O*-methoxyethyluridine (U_{OMOE}), and 2′-*O*-cyanoethyladenine (A_{OCE}) to compare their thermal stabilities. The phosphoramidite of U_{OCE} was synthesized by the ring-opening reaction of 2,2′-anhydrouridine under $BF_3 \cdot OEt_2$, followed by tritylation and phosphorylation.[8] The phosphoramidite building block of U_{OMOE} was synthesized by Reese's method.[42] The phosphoramidite building block of A_{OCE} was prepared by the previously reported procedure.[7]

The oligoribonucleotide synthesis of U_{OMOE} and U_{OCE} was carried out with universal support III (from Glen Research Corp.) and a succinyl linker, respectively. The synthesis of 2′-*O*-cyanoethyluridine-loaded CPG resins was reported previously.[7] To avoid the elimination of the 2′-*O*-cyanoethyl group, the synthesis of an A_{OCE} oligomer was carried out using a silyl linker,[43] which can be cleaved under mild conditions, such as 0.2 M Et_3N-3HF, as shown in Scheme 1. The 2′-*O*-cyanoethyladenosine loaded CPG resin **4** was synthesized by the silylation of compound **1** followed by the deprotection of the fluorenylmethyl group and condensation with amino-loaded CPG by treatment with DCC. Each chain elongation was performed according to the standard procedure of RNA synthesis. Purification of the crude products by anion exchange HPLC gave the homo-oligoribonucleotides (14mer) $U^{OCE}{}_{14}$, $U^{OMOE}{}_{14}$, and $A^{OCE}{}_{14}$. The 2′-*O*-unmodified oligoribonucleotides, $U^{OH}{}_{14}$ and $A^{OH}{}_{14}$, and the 2′-*O*-methylated oligoribonucleotides, $U^{OMe}{}_{14}$, $A^{OMe}{}_{14}$, $(CU)^{OMe}{}_{7}$, and $(AG)^{OMe}{}_{7}$ were purchased as materials purified by HPLC (from Fasmac Co. Ltd.).

UV Melting Temperature Analysis. Next we measured the melting temperature (T_m) of the duplexes. The duplexes of $U^{OH}{}_{14}/A^{OH}{}_{14}$, $U^{OMe}{}_{14}/A^{OH}{}_{14}$, $U^{OMOE}{}_{14}/A^{OH}{}_{14}$, and $U^{OCE}{}_{14}/A^{OH}{}_{14}$ gave T_m values of 24, 36, 40, and 43 °C, respectively (Table 1). The methylation of the 2′-OH group of uridine increased the T_m from 24 to 36 °C (by 12 °C). The introduction of the methoxyethyl (MOE) group gave a much higher T_m of 40 °C, and the cyanoethyl (CE) modified duplex $U^{OCE}{}_{14}/A^{OH}{}_{14}$ gave the highest T_m of 43 °C. Interestingly, the effect of 2′-*O*-modification of the adenosine residues was clearly different from that of uridine residues. The T_m values of $U^{OH}{}_{14}/A^{OH}{}_{14}$, $U^{OH}{}_{14}/A^{OMe}{}_{14}$, and $U^{OH}{}_{14}/A^{OCE}{}_{14}$ were 24, 24, and 27 °C, respectively. In this case, the 2′-*O*-methylation had only negligible effects on the T_m value, and the CE modification also gave a small T_m increase of 3 °C.

Sugar Puckering. The rigidity of sugar puckering has frequently been used to explain the effect of 2′-*O*-modification.[9−11] We tried to clarify the relationship between the rigidity of sugar puckering and the thermal stability of duplexes. The histograms of pseudorotation angles of the modified or unmodified uridine residues in $U^{OH}{}_{14}/A^{OH}{}_{14}$, $U^{OMe}{}_{14}/A^{OH}{}_{14}$, $U^{OMOE}{}_{14}/A^{OH}{}_{14}$, and $U^{OCE}{}_{14}/A^{OH}{}_{14}$ duplexes and the modified and unmodified adenosine residues in $U^{OH}{}_{14}/A^{OH}{}_{14}$, $U^{OH}{}_{14}/A^{OMe}{}_{14}$, and $U^{OH}{}_{14}/A^{OCE}{}_{14}$ duplexes are shown in Figure 3.

As shown in Figure 3a, the pseudorotation angles of the 2′-*O*-modified uridines, such as U_{OMe}, U_{OMOE}, and U_{OCE}, are consistently distributed more sharply than the unmodified uridine residues. However, there was a negligible difference among the 2′-*O*-modified uridines. This tendency was also seen for the adenosine residues, as shown in Figure 3b. The sharpness of the distribution indicates the rigidity of the sugar puckering. These results suggested that the 2′-*O*-modification rigidified the sugar puckering markedly.

The rigidity was quantitatively represented by calculating the elastic constants of sugar puckering. The calculated elastic constants of U_{OH}, U_{OMe}, U_{OCE}, and U_{OMOE} were 3.5, 8.5, 8.6, and 8.5 $cal \cdot mol^{-1} \cdot deg^{-2}$, respectively (Table 1). Larger elastic constant values indicate more rigid structures. Thus, the rigidities of sugar puckering were increased by the 2′-*O*-methylation, methoxyethylation, and cyanoethylation. As mentioned above, there was only a negligible difference among the 2′-*O*-modified uridines. This tendency was also observed for the elastic constants of the adenosine residues. The elastic constants of the pseudorotation angle of A_{OH}, A_{OMe}, and A_{OCE} were 4.4, 7.7, and 7.6 $cal \cdot mol^{-1} \cdot deg^{-2}$, respectively.

Next, we compared these elastic constants and the experimentally determined T_m values. A comparison of the order of the elastic constants and the T_m values suggested that these two parameters did not correlate. For example, the elastic constant of A_{OMe} (7.7 $cal \cdot mol^{-1} \cdot deg^{-2}$) was slightly larger than that of A_{OCE} (7.6 $cal \cdot mol^{-1} \cdot deg^{-2}$). However, the T_m value of A_{OMe} ($U^{OH}{}_{14}/A^{OMe}{}_{14}$, 24 °C) was lower than that of A_{OCE} ($U^{OH}{}_{14}/A^{OCE}{}_{14}$, 27 °C).

Our results indicated that the rigidity of the sugar puckering in the duplex inferred from molecular dynamics did not correlate well with T_m values, at least in the duplexes having 2′-*O*-modification.

Relationship between T_m Values and Elastic Constants of Each Helical Parameter. Then, we analyzed the deformability of the duplexes at the base pair step level. To quantify the deformabilities, we carried out the harmonic stiffness analysis introduced by Lankas et al. and Olson et al.[22−24] The detailed data are shown in Table S1 (Supporting Information).

The plots of the T_m values versus the elastic constants of the six base step parameters showed linear correlations with positive slopes in all cases (Figure 4). These results indicate that more rigid duplexes show higher thermodynamic stabilities. The correlation coefficients for the three translational parameters (rise, shift, and slide) were 0.97, 0.94, and 0.74, respectively, and the other three rotational parameters (twist, roll, and tilt) were 0.89, 0.89, and 0.86, respectively. Among these, the deformability of the rise parameter strongly correlated (R^2 =

SCHEME 1: Preparation of 2′-*O*-Cyanoethyladenosine-Loaded CPG Resin 4[a]

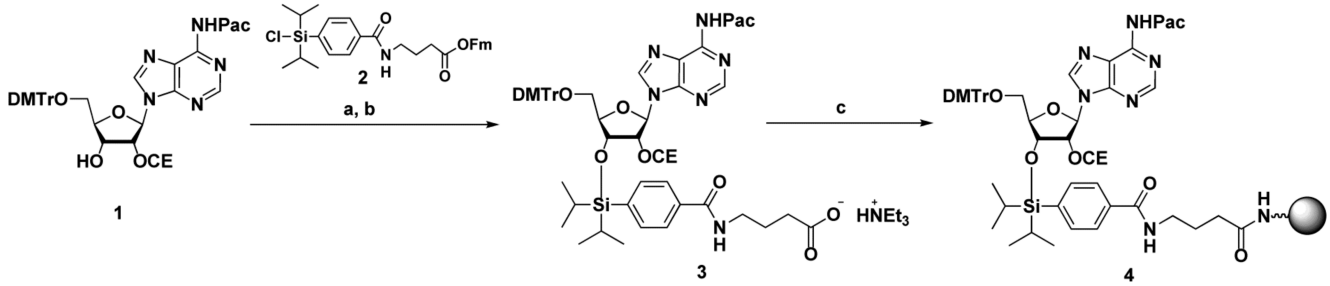

[a] Reagents and conditions: (a) **2**, imidazole, CH_2Cl_2, rt, 1.5 h; (b) DBU, MeCN, rt, 15 min; (c) amino-loaded CPG, DCC, DMAP, CH_2Cl_2, rt, 24 h.

TABLE 1: Elastic Constants of Pseudorotation Angles and T_m Values

	f_{sugar} (cal·mol^{-1}·deg^{-2})	T_m (°C)		f_{sugar} (cal·mol^{-1}·deg^{-2})	T_m (°C)
U_{OH}	3.5[a]	24	A_{OH}	4.4[a]	24
U_{OMe}	8.5[b]	36	A_{OMe}	7.7[e]	24
U_{OCE}	8.6[c]	43	A_{OCE}	7.6[f]	27
U_{OMOE}	8.5[d]	40			

[a] Data were extracted from the $U^{OH}{}_{14}/A^{OH}{}_{14}$ duplexes. [b] Data were extracted from the $U^{OMe}{}_{14}/A^{OH}{}_{14}$ duplexes. [c] Data were extracted from the $U^{OCE}{}_{14}/A^{OH}{}_{14}$ duplexes. [d] Data were extracted from the $U^{OMOE}{}_{14}/A^{OH}{}_{14}$ duplexes. [e] Data were extracted from the $U^{OH}{}_{14}/A^{OMe}{}_{14}$ duplexes. [f] Data were extracted from the $U^{OH}{}_{14}/A^{OCE}{}_{14}$ duplexes.

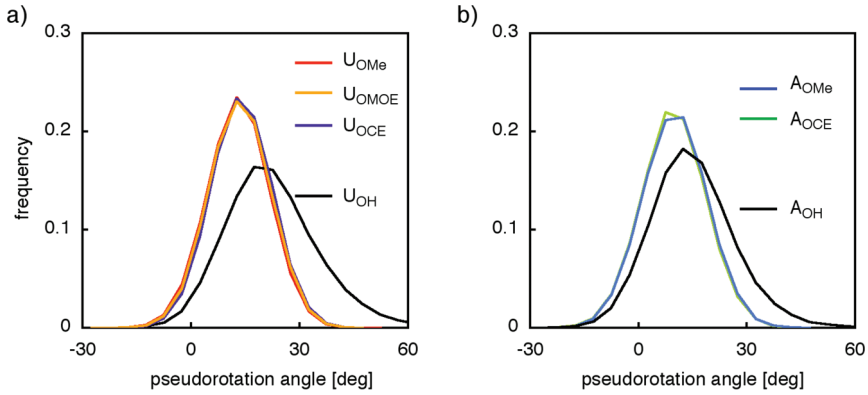

Figure 3. Histograms of pseudorotation angles. (a) Modified or unmodified uridine residues in $U^{OH}{}_{14}/A^{OH}{}_{14}$, $U^{OMe}{}_{14}/A^{OH}{}_{14}$, $U^{OMOE}{}_{14}/A^{OH}{}_{14}$, and $U^{OCE}{}_{14}/A^{OH}{}_{14}$ duplexes. (b) Modified or unmodified adenosine residues in $U^{OH}{}_{14}/A^{OH}{}_{14}$, $U^{OH}{}_{14}/A^{OMe}{}_{14}$, and $U^{OH}{}_{14}/A^{OCE}{}_{14}$ duplexes.

0.97) with the T_m values. This observation suggests that the rise parameter is the most useful indicator for predicting the T_m value as long as each helical parameter is considered separately.

Relationship between T_m Values and Global Elastic Constants of Helical Parameters. Next, we calculated the elastic constants of translation (F_{trans}), rotation (F_{rot}), and their product deformability ($F_{prod} = F_{trans} \times F_{rot}$) and compared them with the T_m values. Detailed data are shown in Table S2 (Supporting Information). The plot of T_m values showed strong correlation with F_{trans}, F_{rot}, and F_{prod} constants (Figure 5). The correlation coefficients of F_{trans}, F_{rot}, and F_{prod} are 0.96, 0.92, and 0.98, respectively. Among these three coefficients, F_{prod} had the largest correlation efficient.

The strong correlation of F_{prod} with T_m values indicates the importance of considering the product deformability for estimation of the thermal stability. To predict the thermal stability using this correlation, we calculated the linear approximation equation by the least-squares method. The linear approximation equation of F_{prod} and T_m values is given by

$$T_m = 3957 \times F_{prod} + 17.4 \quad (1)$$

This equation can be used only for the A_{14}/U_{14}-type duplex discussed in this paper. The data of the experimental and predicted T_m values are shown in Table 2. The calculated T_m values (and experimental T_m in parentheses) were 22.0 °C (24 °C) for $U^{OH}{}_{14}/A^{OH}{}_{14}$, 35.0 °C (36 °C) for $U^{OMe}{}_{14}/A^{OH}{}_{14}$, 40.1 °C (40 °C) for $U^{OMOE}{}_{14}/A^{OH}{}_{14}$, 43.2 °C (43 °C) for $U^{OCE}{}_{14}/A^{OH}{}_{14}$, 24.7 °C (24 °C) for $U^{OH}{}_{14}/A^{OMe}{}_{14}$, and 28.7 °C (27 °C) for $U^{OH}{}_{14}/A^{OCE}{}_{14}$. The discrepancies between experimental and the calculated data were −2.0 to +1.7 °C for the A_{14}/U_{14}-type duplexes.

Deformability Analyses for Duplexes Having Mixed Sequences. Next, we studied the relationship that more rigid structures showed higher T_m values by using 2′-*O*-modified hetero duplexes having mixed sequences. For the analyses of mixed sequences we tried to parametrize the deformability (F_{prod}) of each base-pair steps, 5′-N^1N^2-3′/3′-$\underline{N^3N^4}$-5′, where N and $\underline{N}$ represented either 2′-*O*-modified or unmodified nucleotide residues. For example, for the parametrization of the 2′-*O*-methyl-RNA/RNA duplex we have to obtain sixteen parameters of the 5′-N^1N^2-3′/3′-$\underline{N^3N^4}$-5′ base steps, where N^1 and N^2

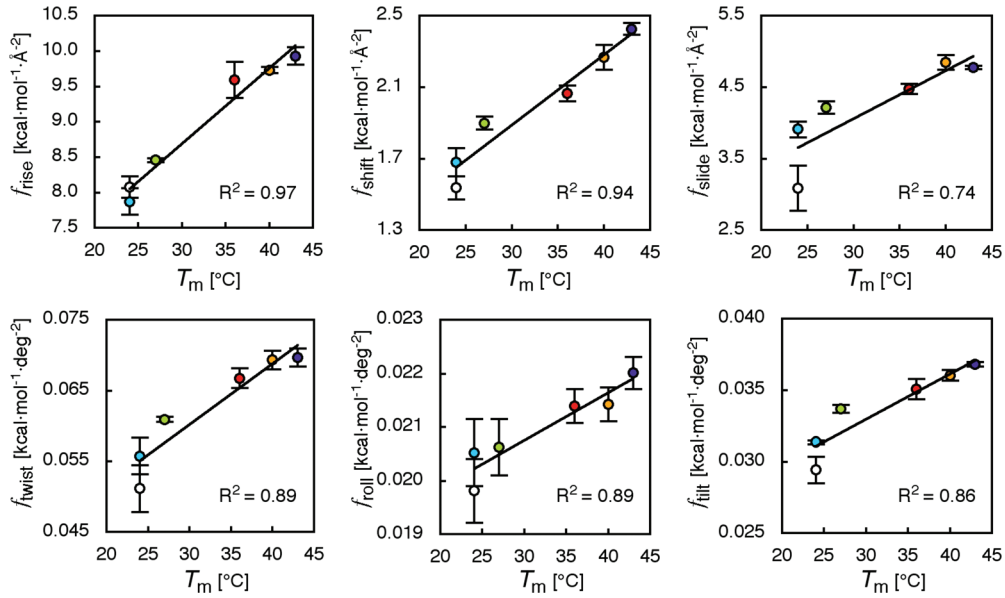

Figure 4. Correlations between the T_m values versus elastic constant of each helical parameter. The circles refer to $U^{OH}{}_{14}/A^{OH}{}_{14}$ (white), $U^{OMe}{}_{14}/A^{OH}{}_{14}$ (red), $U^{OMOE}{}_{14}/A^{OH}{}_{14}$ (orange), $U^{OCE}{}_{14}/A^{OH}{}_{14}$ (purple), $U^{OH}{}_{14}/A^{OMe}{}_{14}$ (blue), and $U^{OH}{}_{14}/A^{OCE}{}_{14}$(green).

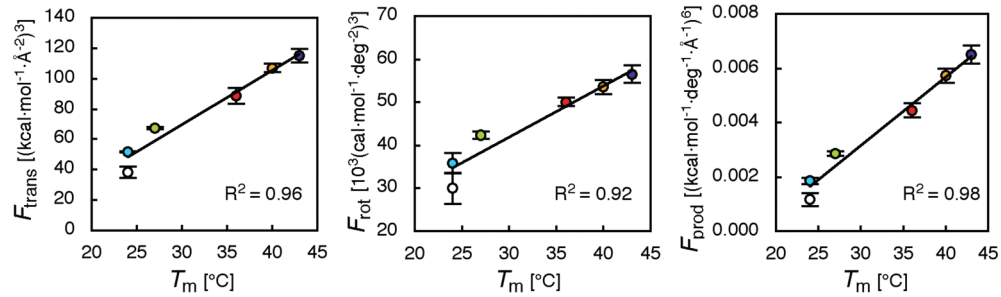

Figure 5. Correlations between T_m values versus F_{trans}, F_{rot}, or F_{prod} values. The circles refer to $U^{OH}{}_{14}/A^{OH}{}_{14}$ (white), $U^{OMe}{}_{14}/A^{OH}{}_{14}$ (red), $U^{OMOE}{}_{14}/A^{OH}{}_{14}$ (orange), $U^{OCE}{}_{14}/A^{OH}{}_{14}$ (purple), $U^{OH}{}_{14}/A^{OMe}{}_{14}$ (blue), and $U^{OH}{}_{14}/A^{OCE}{}_{14}$ (green).

TABLE 2: Comparison of Experimental and Calculated T_m Values

duplex	F_{prod} [(kcal·mol^{-1}·deg^{-1}·Å^{-1})^6]	T_m(exp) (°C)	T_m(calc) (°C)	$\Delta T_m{}^a$ (°C)
$U^{OH}{}_{14}/A^{OH}{}_{14}$	0.00116 ± 0.00024	24	22.0	−2.0
$U^{OMe}{}_{14}/A^{OH}{}_{14}$	0.00445 ± 0.00026	36	35.0	−1.0
$U^{OMOE}{}_{14}/A^{OH}{}_{14}$	0.00573 ± 0.00026	40	40.1	0.1
$U^{OCE}{}_{14}/A^{OH}{}_{14}$	0.00651 ± 0.00034	43	43.2	0.2
$U^{OH}{}_{14}/A^{OMe}{}_{14}$	0.00185 ±0.00012	24	24.7	0.7
$U^{OH}{}_{14}/A^{OCE}{}_{14}$	0.00286 ± 0.00009	27	28.7	1.7

[a] $\Delta T_m = T_m(\text{calc}) - T_m(\text{exp})$.

represent A, U, G, or C and $\underline{N}^3$ and $\underline{N}^4$ represented 2′-*O*-methyl-A, -U, -G, or -C.

To obtain the parameters, we carried out the MD simulations and the deformability analyses by using Seq1: $(UUAA)_5UUA/(UAAU)_5UAA$, Seq2: $(CCGG)_5CCG/(CGGC)_5CGG$, and Seq3: $(ACUG)_5ACU/(AGUC)_5AGU$ base sequences. By using the data for Seq1, we can obtain the F_{prod} of 5′-AA-3′/3′-$\underline{UU}$-5′, 5′-AU-3′/3′-$\underline{UA}$-5′, 5′-UA-3′/3′-$\underline{AU}$-5′, and 5′-UU-3′/3′-$\underline{AA}$-5′. In addition, by using Seq2 and Seq3, we can obtain the F_{prod} for all base pair steps. We defined a new parameter "total stiffness index (F_{total})" as the sum of F_{prod}. The calculated F_{prod} value of each base pair step was shown in Table S4 (Supporting Information).

To verify the linear assumption between the melting temperature and the total stiffness index (F_{total}), the F_{total} values of 14mer duplexes $((CU)^{OH}{}_7/(AG)^{OH}{}_7$, $(CU)^{OMe}{}_7/(AG)^{OH}{}_7$, $(CU)^{OH}{}_7/(AG)^{OMe}{}_7)$ and 12mer duplexes $((GACU)^{OH}{}_3/(AGUC)^{OH}{}_3$, $(GACU)^{OMe}{}_3/(AGUC)^{OH}{}_3$, $(GACU)^{OCE}{}_3/(AGUC)^{OH}{}_3)$ were plotted against the experimentally determined T_m values (Figure 6). The detailed F_{total}, calculated and experimental T_m values are shown in the Supporting Information (Table S5).

Surprisingly, even in the mixed sequences, the T_m values were found to correlate well with the F_{total} values, which were only the sums of the F_{prod} value of each base-pair step. The correlation coefficient of a GACU sequence was 0.97 and that of a CU sequence was 0.99. Thus, the deformability analyses could be expanded to the duplexes with mixed sequences by introducing new parameter F_{total}.

Discussion

In this paper we presented the deformability analysis for U_{14}/A_{14} and mixed sequences. These results indicated that deformability is a good indicator for the estimation of the thermal

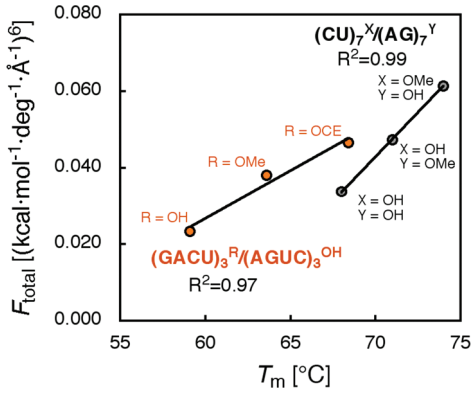

Figure 6. Correlations between T_m values versus F_{total} values in $(GACU)_3/(AGUC)_3$ and $(CU)_7/(AG)_7$ sequence. The data of CU sequence are $(CU)^{OH}{}_7/(AG)^{OH}{}_7$, $(CU)^{OMe}{}_7/(AG)^{OH}{}_7$, and $(CU)^{OH}{}_7/(AG)^{OMe}{}_7$. The data of GACU sequence are $(GACU)^{OH}{}_3/(AGUC)^{OH}{}_3$, $(GACU)^{OMe}{}_3/(AGUC)^{OH}{}_3$, and $(GACU)^{OCE}{}_3/(AGUC)^{OH}{}_3$ (Table S5, Supporting Information).

stability of 2′-*O*-modified RNAs. Although the deformability predicted the T_m values well, the contributions of the physicochemical factors such as hydrogen bonds, stacking interactions, conformational rigidity, and hydration effects to the deformabilities have not been well understood. However, some plausible relationships between the physicochemical factors and deformabilities could be hypothesized. As previously reported, the conformational effect of sugar puckering on uridine nucleotide by 2′-*O*-methylation is commonly explained by the steric repulsion between the 2-carbonyl group and the 2′-*O*-methyl group.[9] The weak effect of 2′-*O*-methylation on the fluctuation of the adenine base could be explained by the lack of this type of steric repulsion. In the case of the sequences incorporating 2′-*O*-methyl-pyrimidine nucleosides, the rigidity of the sugar conformation might reflect the large F_{total} value.

Moreover, the 2′-*O*-methylation also stabilizes hydrated waters in the minor groove.[17] If the water molecules in the minor groove were stabilized so that they could remain unmoved for a long time, it could reduce the fluctuation of the base-pair steps. Thus, the stabilization of the hydration by the 2′-*O*-methylation could also contribute to the large F_{total}.

These explanations also raised the limitation of this method. First, the modifications that affected the electrostatic repulsion among phosphate groups, such as modifications with positive or negative charges, would not be estimated well because the change of the electrostatic repulsion could increase or decrease the duplex stability without affecting the deformability. In addition, since our method was only derived from the calculations at the duplex states, care should be taken for the modifications that can drastically change the properties of the single strand states. BNA or LNA, which has perfectly fixed sugar moieties even in the single strand, is an example.

Furthermore, the linear functions of the deformability and T_m values are different among base sequences (Figure 6, Table S5 (Supporting Information)). This would mean that our method cannot be used for comparable study between the duplexes of different base sequences. Therefore, in practice, one must measure the experimental values of at least two modified or unmodified duplexes of each targeted base sequence.

It should be also noted that it was also difficult to explain the deformability from the aspect of entropy or enthalpy contributions (Figure S6, Supporting Information). These analyses indicated that the more rigid base pair steps did not necessarily mean the base pair steps of the lower entropy state. Despite the lack of rationale for the correlation, it is clear that the deformability analysis is able to estimate the relative stability of RNA duplexes incorporating 2′-OH, OMe, OCE, and OMOE derivatives of ribonucleosides. The deformability analysis was still not a perfect indicator of the predicting the thermal stability of 2′-*O*-modified duplexes, but it showed possibility of predicting the thermal stability at the computer-aided molecular design stage.

Conclusion

We introduced two parameters (F_{prod} and F_{total}) and found strong correlations with the melting temperatures. The correlation would be used for the linear prediction of the T_m values within ±2.0 °C. We showed here the possibility of predicting a change in thermal stability by 2′-*O*-modification. In addition, this deformability analysis can also be used for biologically useful 2′-*O*-modified designs having an appropriate thermal stability.

Experimental Section

General Remarks. ^{1}H spectra were recorded at 500 MHz NMR. The chemical shifts were measured from $CDCl_3$ (7.26 ppm). UV spectra were recorded with a U-2000 spectrometer. Column chromatography was performed with silica gel C-200 (purchased from Wako Co. Ltd.). High performance liquid chromatography (HPLC) was performed using the following systems: Reversed exchange HPLC was done on a Waters Alliance system with a Waters 3D UV detector and a Waters XTerra MS C18 column (4.6 × 150 mm); a linear gradient (0−30%) of solvent I [0.1 M ammonium acetate buffer (pH 7.0)] in solvent II (CH_3CN) was used at 50 °C at a flow rate of 1.0 mL/min for 30 min; anion-exchange HPLC was done on a Shimadzu LC-10 AD VP with a Shimadzu 3D UV detector and a Gen-Pak FAX column (Waters, 4.6 × 100 mm); a linear gradient (10−67%) of solvent III [1 M NaCl in 25 mM phosphate buffer (pH 6.0)] in solvent IV [25 mM phosphate buffer (pH 6.0)] was used at 50 °C at a flow rate of 1.0 mL/min for 40 min. ESI mass was performed by use of Mariner (PerSeptive Biosystems Inc.). MALDI-TOF mass was performed using a Bruker Daltonics [Matrix: 3-hydoroxypicolinic acid (100 mg/mL) in H_2O−diammonium hydrogen citrate (100 mg/mL) in H_2O (10:1, v/v)].

Synthesis of Compound 3. 6-*N*-Phenoxyacetyl-5′-*O*-(4,4′-dimethoxytrityl)-2′-*O*-cyanoethyladenosine (**1**) (0.25 g, 0.33 mmol) and imidazole (0.13 g, 1.83 mmol) in CH_2Cl_2 (1.65 mL) were added to the solution of compound **2** (0.37 mmol) in CH_2Cl_2 (1.85 mL) under an argon atmosphere. After the mixture was stirred at room temperature for 90 min, the mixture was partitioned between $CHCl_3$ and brine. The organic phase was collected and evaporated under reduced pressure. The residue was chromatographed on a column of silica gel with $CHCl_3$ containing 1% Et_3N to give the fractions containing the desired silylated nucleoside. The fractions were collected and evaporated under reduced pressure. The residue was finally evaporated by repeated coevaporation three times with toluene and $CHCl_3$ to remove the last traces of Et_3N. Subsequently, the residue was dissolved in dry CH_3CN (2.8 mL). 1,8-Diazabicyclo[5.4.0]-7-undecene (170 μL, 1.13 mmol) was added to the mixture. After the mixture was stirred at room temperature for 15 min, a 0.2 M solution of triethylamine hydrogen carbonte (1.4 mL) was added. After being stirred at room temperature for 5 min, the mixture was partitioned between $CHCl_3$ and brine. The organic phase was collected and evaporated under reduced pressure. The residue was chromatographed on a column of silica gel with

$CHCl_3$−MeOH (100:0−95:5, v/v) containing 1% Et_3N. The fractions were collected and evaporated under reduced pressure. The residue was finally evaporated by repeated coevaporation three times with toluene and $CHCl_3$ to give compound **3** (0.25 g, 64%). ^{1}H NMR ($CDCl_3$): δ 0.92 (d, 3H, J = 7.5 Hz), 0.94 (d, 3H, J = 8.0 Hz), 1.00 (d, 3H, J = 7.5 Hz), 1.02 (d, 3H, J = 8.0 Hz), 1.04−1.16 (m, 1H), 1.28−1.32 (m, 3H), 1.95−2.06 (br s, 2H), 2.50−2.57 (m, 2H), 2.57−2.62 (br s, 2H), 3.23 (d, 1H, J = 10.0 Hz), 3.49−3.68 (m, 4H), 3.70−3.82 (m, 8H), 4.31−4.38 (br s, 1H), 4.48 (s, 1H), 4.70−4.77 (br s, 1H), 4.81 (s, 1H), 6.18 (s, 1H), 6.72−6.82 (br s, 4H), 7.01−7.10 (m, 3H), 7.15−7.25 (m, 6H), 7.29−7.40 (m, 4H), 7.55−7.61 (m, 3H), 7.78 (d, 2H, J = 8.0 Hz), 8.17 (s, 1H), 8.74 (s, 1H), 9.46−9.47 (brs, 1H). HRMS (ESI) m/z (M + H) calcd for $C_{59}H_{66}N_7O_{11}Si^+$: 1076.4584. Found: 1076.4580.

Synthesis of Compound 4. A CPG resin (1 g, 20 μmol) was coevaporated with dry pyridine three times and dried under reduced pressure. The CPG resin was added in dry CH_2Cl_2 (10 mL) in a round flask; compound **3** and DCC (0.1 g, 500 μmol) were added to the mixture. After the round flask containing the mixture was attached to a rotary evaporator and gently rotated for 12 h, the solvent was removed by filtration. The residual CPG was washed by CH_2Cl_2 and dried under reduced pressure. The resin was then dissolved in pyridine−Ac_2O (9:1, v/v, 30 mL) in a round flask and 4-(dimethylamino)pyridine (80 mg, 640 μmol) was added. The round flask containing the mixture was attached to a rotary evaporator and gently rotated for 2 h, and the solvent was removed by filtration. The residual CPG resin **4** was washed with CH_3CN and dried under reduced pressure.

Synthesis of Oligoribonucleotides. The synthesis of oligoribonucleotides $U^{OMOE}{}_{14}$ and $U^{OCE}{}_{14}$ was carried out on a CPG resin having a universal support III and a succinyl linker in an ABI 392 DNA synthesizer, respectively. Then, the $U^{OMOE}{}_{14}$ and $U^{OCE}{}_{14}$ oligomers were released from the resin by treatment with a solution of 2.0 M methanolic ammonium and aqueous NH_3−NH_4OAc (10:1, v/w) solution, respectively, at room temperature for 1 h. The polymer supports were removed by filtration and washed with 0.1 M ammonium acetate buffer (1 mL × 3). The filtrates were purified by anion-exchange HPLC to give oligoribonucleotides $U^{OMOE}{}_{14}$ and $U^{OCE}{}_{14}$. The synthesis of oligoribonucleotides $A^{OCE}{}_{14}$ was carried out on a CPG resin having a silyl linker in an ABI 392 DNA synthesizer. The fully protected oligomer, after chain elongation, was deprotected by treatment with an aqueous NH_3−NH_4OAc (10:1, v/w) solution at room temperature for 45 min. Then, the mixture containing oligoRNAs was released from the resin by treatment with a solution of $Et_3N\cdot 3HF$ (0.2 M) and Et_3N (0.4 M) in THF (500 μL) at room temperature for 4 h. The polymer support was removed by filtration and washed with 0.1 M ammonium acetate buffer (1 mL × 3). The filtrate was purified by anion-exchange HPLC to give oligoribonucleotides.

Oligoribonucleotide: $A^{OCE}{}_{14}$

MALDI-TOF Mass (M + H) calcd for $C_{183}H_{214}N_{84}O_{81}P_{13}{}^+$: 5286.2;. Found: 5291.2.

Oligoribonucleotide: $U^{OCE}{}_{14}$

MALDI-TOF Mass (M + H) calcd for $C_{168}H_{198}N_{42}O_{110}P_{13}{}^+$: 4965.8. Found: 4970.4.

Oligoribonucleotide: $U^{OMOE}{}_{14}$

MALDI-TOF Mass (M + H) calcd for $C_{168}H_{240}N_{28}O_{124}P_{13}{}^+$: 5036.0. Found: 5036.5.

UV Melting Curve Analysis. An appropriate oligoribonucleotide (2 μM) and its complementary ssRNA (2 μM) were dissolved in a buffer consisting of 100 mM NaCl, 10 mM sodium phosphate, and 0.1 mM EDTA adjusted to pH 7.0. The solution was kept at 85 °C for 10 min for complete dissociation of the duplex to single strands, cooled at a rate of 1.0 °C/min and kept at 15 °C for 10 min. After that, the melting temperatures (T_m) were determined at 260 nm using a UV spectrometer (Pharma Spec UV-1700^{TM}, Shimadzu) by increasing the temperature at a rate of 1.0 °C/min.

Computational Methods. The simulations were carried out using the AMBER 9.0 program package with the parmBSC0 revision of the parm99 Cornell et al. force field.[31,32] The initial structures of each duplex were derived from NUCGEN module embedded in AMBER. The charge of the 2′-*O*-methyl group (2′-OMe) was taken from the Auffinger's parameter.[17] Parameterization of the 2′-*O*-cyanoethyl (2′-OCE) and 2′-*O*-methoxyethyl (2′-OMOE) groups was done using the RESP/6-31G(d) charges.[33−35] The additional force field parameters of the 2′-OCE group were taken from the gaff force-field parameters.[36]

The sequence of calculated 2′-*O*-modified-RNA/RNA hetero duplexes were U_{14}/A_{14}, $(UUAA)_5UUA/(UAAU)_5UAA$, $(CCGG)_5CCG/(CGGC)_5CGG$, and $(ACUG)_5ACU/(AGUC)_5AGU$. The RNAs were solvated in a periodic box with a 10 Å buffer of water molecules, explicitly described by the SPC/E model and neutralized, resulting in a concentration of added NaCl of approximately 0.1 M.[37] The parameters included in ions94.lib file embedded in AMBER 9.0 were used for Na^+ and Cl^- ions. An initial optimization of 1000 cycles, the first 500 cycles by steepest descent and the rest with a conjugate gradient method, was performed with the duplex constrained 500 kcal/(mol·Å^2) to relax the solvent. Then, a further optimization of 5000 cycles with no constraints on the whole system was carried out to lead to a final relaxed geometry. The first equilibrations were carried out with a 10 kcal/(mol·Å^2) constraint on the duplex for 100 ps at constant volume, constantly increasing the temperature from 0 to 300 K. Next, the equilibrations were continued to 200 ps at a constant pressure of 1 atm, and the temperature was kept constant with the Langevin algorithm. The production simulations were performed for 25 ns (U_{14}/A_{14}) or 20 ns (the others) with the Berendsen algorithm to maintain the temperature.[38] The time constant (1.0 ps) for the heat bath coupling was used. During the MD calculation, hydrogen vibrations were removed using SHAKE bond constraints, allowing a longer time step of 2 fs.[39] Long range electrostatic interactions were treated using the particle mesh Ewald approach and a 10 Å cutoff.[40]

Harmonic Stiffness Analysis. Harmonic stiffness analysis for the helical parameters of nucleic acids, such as twist, roll, tilt, rise, shift and slide, was introduced by Lankas et al. and Olson et al. to quantitatively analyze the deformability of nucleic acid duplexes.[22−24] The harmonic stiffness analysis is based on the identical form of the Gauss distribution function (eq 2) and Einstein's formula of a harmonic oscillator (eq 3).

$$P(x) = N\exp\left(-\frac{(x-\mu)^2}{2\sigma^2}\right) \quad (2)$$

$$P(x) = N\exp\left(-\frac{f(x-\mu)^2}{2}\cdot\frac{1}{k_BT}\right) \quad (3)$$

where x is any structural parameter, μ is the average of x, σ is the standard deviation, f is the elastic constant, N is the normalization constant, k_B is Boltzmann's constant, and T is the absolute temperature, respectively. In the simple case, by comparing these two formulas, one can calculate the f value as (eq 4) from the standard deviation (σ) obtained by analyzing

the distribution of parameter x throughout the molecular dynamic simulation.

$$f = \frac{k_B T}{\sigma^2} \tag{4}$$

In complex molecules, such as DNA duplexes, each of the structural parameters, such as roll, rise, shift, slide, tilt, and twist, are correlated. Therefore, a covariance−variance matrix (C) of six parameters (twist, roll, tilt, rise, shift, and slide) was used instead of the σ^2 value.

$$F = k_B T C^{-1} \tag{5}$$

where F is the stiffness matrix associated with helical deformation at the base pair step.

A global view of helical deformability can be obtained by defining the translational (F_{trans}), rotational (F_{rot}), and their product (F_{prod}) deformability indexes.[25]

$$F_{\text{trans}} = f_{\text{rise}} f_{\text{shift}} f_{\text{slide}} \tag{6}$$

$$F_{\text{rot}} = f_{\text{twist}} f_{\text{roll}} f_{\text{tilt}} \tag{7}$$

$$F_{\text{prod}} = F_{\text{trans}} F_{\text{rot}} \tag{8}$$

For the analyses of mixed sequences, we tried to parametrize the deformability of each base-pair step, 5′-N^1N^2-3′/3′-$\underline{N}^3\underline{N}^4$-5′, where N and $\underline{N}$ represented either 2′-modified or unmodified nucleotide residues. We defined a new parameter "total stiffness index (F_{total})" as the sum of F_{prod}.

$$F_{\text{total}} = \Sigma F_{\text{prod}} \tag{9}$$

In this study, the molecular dynamics simulations were analyzed using Ptraj modules of AMBER 9.0, and X3DNA.[41] The elastic constants (f) could be calculated under harmonic approximation, as described above.[22−24]

The elastic constant of sugar puckering was obtained by using eq 4. The stiffness matrix (F) associated with helical deformation at the base pair step was determined as the inverse of the covariance-variance matrix (C) of six parameters (twist, roll, tilt, rise, shift, and slide), which were extracted by X3DNA.[40] The diagonal elements of the stiffness matrix were used as the elastic constants of the helical parameters.

We used the three 5 ns data extracted from last 15 ns of the 25.3 ns trajectory for the U_{14}/A_{14} system. Thus, the error bars shown in Figures 4 and 5 are the standard deviations determined from 10.3−15.3, 15.3−20.3, and 20.3−25.3 ns data. To obtain the F_{prod} of each base-pair step for mixed sequences, we carried out 20.3 ns MD simulations for Seq1: $(UUAA)_5UUA/(UAAU)_5UAA$, Seq2: $(CCGG)_5CCG/(CGGC)_5CGG$, and Seq3: $(ACUG)_5ACU/(AGUC)_5AGU$ base sequences. By using the data for Seq1, we can obtain the deformability parameters of 5′-UU-3′/3′-$\underline{AA}$-5′, 5′-UA-3′/3′-$\underline{AU}$-5′, 5′-AA-3′/3′-$\underline{UU}$-5′, and 5′-AU-3′/3′-$\underline{UA}$-5′ base pair steps. In addition, by using the Seq2 and Seq3, we can obtain the parameters for all base pair steps. The data of the last 10 ns were analyzed for these 23mer sequences. We analyzed the parameters of only the central base pairs (omitting terminal 3 base pairs) and averaged same base pair steps to provide more reliable values.

Acknowledgment. This study was supported in part by a grant from the Genome Network Project from the Ministry of Education, Culture, Sports, Science and Technology, Japan, and by the G-COE project. This study was also supported in part by a KAKENHI 20350074 from the Ministry of Education, Culture, Sports, Science, and Technology, Japan, and Research for Promoting Technological Seeds program of JST.

Supporting Information Available: Detailed RESP charges and force field parameters of modified moiety, base-pair step data, rms deviation of each trajectory, and realtionship between deformability and thermodynamic parameter. This material is available free of charge via the Internet at http://pubs.acs.org.

References and Notes

(1) Soutschek, J.; Akinc, A.; Bramlage, B.; Charisse, K.; Constien, R.; Donoghue, M.; Elbashir, S.; Geick, A.; Hadwiger, P.; Harborth, J.; John, M.; Kesavan, V.; Lavine, G.; Pandey, R. K.; Racie, T.; Rajeev, K. G.; Rohl, I.; Toudjarska, I.; Wang, G.; Wuschko, S.; Bumcrot, D.; Koteliansky, V.; Limmer, S.; Manoharan, M.; Vornlocher, H. P. *Nature* **2004**, *432*, 173–178.

(2) Prakash, T. P.; Kawasaki, A. M.; Wancewicz, E. V.; Shen, L.; Monia, B. P.; Ross, B. S.; Bhat, B.; Manoharan, M. *J. Med. Chem.* **2008**, *51*, 2766–2776.

(3) Egli, M.; Minasov, G.; Tereshko, V.; Pallan, P. S.; Teplova, M.; Inamati, G. B.; Lesnik, E. A.; Owens, S. R.; Ross, B. S.; Prakash, T. P.; Manoharan, M. *Biochemistry* **2005**, *44*, 9045–9057.

(4) Honcharenko, D.; Barman, J.; Varghese, O. P.; Chattopadhyaya, J. *Biochemistry* **2007**, *46*, 5635–5646.

(5) Davis, S.; Lollo, B.; Freier, S.; Esau, C. *Nucleic Acids Res.* **2006**, *34*, 2294–2304.

(6) Kawasaki, A. M.; Casper, M. D.; Freier, S. M.; Lesnik, E. A.; Zounes, M. C.; Cummins, L. L.; Gonzalez, C.; Cook, P. D. *J. Med. Chem.* **1993**, *36*, 831–841.

(7) Saneyoshi, H.; Seio, K.; Sekine, M. *J. Org. Chem.* **2005**, *70*, 10453–10460.

(8) Saneyoshi, H.; Okamoto, I.; Masaki, Y.; Ohkubo, A.; Seio, K.; Sekine, M. *Tetrahedron Lett.* **2007**, *48*, 8554–8557.

(9) Kawai, G.; Yamamoto, Y.; Kamimura, T.; Masegi, T.; Sekine, M.; Hata, T.; Limori, T.; Watanabe, T.; Miyazawa, T; Yokoyama, S. *Biochemistry* **1992**, *31*, 1040–1046.

(10) Cheng, D. M.; Sarma, R. H. *Biopolymers* **1977**, *16*, 1687–1711.

(11) Barbe, S.; Bret, M. L. *J. Phys. Chem. A* **2008**, *112*, 989–999.

(12) Yathindra, N.; Sundaralingam, M. *Biopolymers* **1979**, *18*, 2721–2731.

(13) Lubini, P.; Zurcher, W.; Egli, M. *Chem. Biol.* **1994**, *1*, 39–45.

(14) Bobst, A. M.; Rottman, F.; Cerutti, P. A. *J. Mol. Biol.* **1969**, *46*, 221–234.

(15) Drake, A. F.; Mason, S. F.; Trim, A. R. *J. Mol. Biol.* **1974**, *86*, 727–739.

(16) Singh, H.; Herbut, M. H.; Lee, C. H.; Sarma, R. H. *Biopolymers* **1976**, *15*, 2167–2184.

(17) Auffinger, P.; Westhof, E. *Angew. Chem., Int. Ed.* **2001**, *40*, 4648–4650.

(18) Rozners, E.; Moulder, J. *Nucleic Acids Res.* **2004**, *32*, 248–254.

(19) Venkateswarlu, D.; Lind, E. K.; Mohan, V.; Manoharan, M.; Ferguson, D. M. *Nucleic Acids Res.* **1999**, *27*, 2189–2195.

(20) Kierzek, E.; Mathews, D. H.; Ciesielska, A.; Turner, D. H.; Kierzek, R. *Nucleic Acids Res.* **2006**, *34*, 3609–3614.

(21) Kool, E. *Chem. Rev.* **1997**, *97*, 1473–1488.

(22) Olson, W. K.; Gorin, A. A.; Lu, X. J.; Hock, L. M.; Zhurkin, V. B. *Proc. Natl. Acad. Sci. U.S.A.* **1998**, *95*, 11163–11168.

(23) Lankas, F.; Sponer, J.; Langowski, J.; Cheatham, T. E., III. *Biophys. J.* **2003**, *85*, 2872–2883.

(24) Lankas, F. *Biopolymers* **2004**, *73*, 327–339.

(25) Noy, A.; Luque, F. J.; Orozco, M. *J. Am. Chem. Soc.* **2008**, *130*, 3486–3496.

(26) Réblová, K.; Lankas, F.; Rázga, F.; Krasovska, M. V.; Koca, J.; Sponer, J. *Biopolymers* **2006**, *82*, 504–520.

(27) Fujii, S.; Kono, H.; Takenaka, S.; Go, N.; Sarai, A. *Nucleic Acids Res.* **2007**, *35*, 6063–6074.

(28) Anselmi, C.; Bocchinfuso, G.; Santis, P. D.; Savino, M.; Scipioni, A. *Biophys. J.* **2000**, *79*, 601–613.

(29) Anselmi, C.; Santis, P. D.; Paparcone, R.; Savino, M.; Scipioni, A. *Biophys. Chem.* **2002**, *95*, 23–47.

(30) Scipioni, A.; Anselmi, C.; Zuccheri, G.; Samori, B.; Santis, P. D. *Biophys. J.* **2002**, *83*, 2408–2418.
(31) Cheatham, T. E., III; Cieplak, P.; Kollman, P. A. *J. Biomol. Struct. Dyn.* **1999**, *16*, 845–862.
(32) Perez, A.; Marchan, I.; Svozil, D.; Sponer, J.; Cheatham, T. E., III; Laughton, C. A.; Orozco, M. *Biophys. J.* **2007**, *92*, 3817–3829.
(33) Bayly, C. I.; Cieplak, P.; Cornell, W.; Kollman, P. A. *J. Phys. Chem.* **1993**, *97*, 10269–10280.
(34) Aduri, R.; Psciuk, B. T.; Saro, P.; Taniga, H.; Schlegel, H. B.; Santa Lucia, J., Jr. *J. Chem. Theory and Comput.* **2007**, *3*, 1464–1475.
(35) Zhang, Q.; Schlick, T. *Biophys. J.* **2006**, *90*, 1865–1877.
(36) Wang, J.; Wolf, R. M.; Caldwell, J. W.; Kollman, P. A.; Case, D. A. *J. Comput. Chem.* **2004**, *25*, 1157–1174.
(37) Berendsen, H. J. C.; Grigera, J. R.; Straatsma, T. P. *J. Phys. Chem.* **1987**, *91*, 6269–6271.
(38) Berendsen, H. J. C.; Postma, J. P. M.; van Gunsteren, W. F.; DiNola, A.; Haak, J. R. *J. Chem. Phys.* **1984**, *81*, 3684–3690.
(39) Ryckaert, J. P.; Ciccotti, G.; Berendsen, H. J. C. *J. Comput. Phys.* **1977**, *23*, 327–341.
(40) Darden, T.; York, D.; Pedersen, L. *J. Chem. Phys.* **1993**, *98*, 10089–10092.
(41) Lu, X. J.; Olson, W. K. *Nucleic Acids Res.* **2003**, *31*, 5108–5121.
(42) Legorburu, U.; Reese, C. B.; Song, Q. *Tetrahedron* **1999**, *55*, 5635–5640.
(43) Ohkubo, A.; Kasuya, R.; Aoki, K.; Kobori, A.; Taguchi, H.; Seio, K.; Sekine, M. *Bioorg. Med. Chem.* **2008**, *16*, 5345–5351.

JP909851J